Supplementary Information:

Semi-Transparent Perovskite Films with Centimeter-Scale Superior Uniformity by the Hybrid Deposition Method

Luis K. Ono [1], Shenghao Wang [1], Yuichi Kato, Sonia R. Raga, Yabing Qi*
Energy Materials and Surface Sciences Unit, Okinawa Institute of Science and Technology Graduate University, 1919-1 Tancha Onna-son, Okinawa 904-0495 Japan.
*E-mail: yabing.qi@oist.jp
[1] Luis K. Ono and Shenghao Wang contributed equally to this work.

Contents:

Experimental Section.

Instrumentation details. The overall side-view of the hybrid deposition system is displayed in Fig. 1a and S1. Additional top-views at the different cross sections of the instrument are displayed in Fig. S1. The main vacuum chamber (customized system, Part #1 in Fig. 1a) is evacuated by a pumping system (Part #2) which consists of a turbo molecular pump (HiPace300, Pfeiffer), manual gate-valve (10840-CE01, VAT). The substrate holder stage (Part #3) allows stable cooling and heating in the temperature range from −190°C up to 200°C. The system can accommodate a wide range of substrate (Part #4) sizes (up to 5 cm×5 cm). The substrate shutter (Part #5) is mounted on a push-pull linear motion device (MDC) just below the substrate. The evaporation rates are monitored by two QCMs (Inficon, Parts #6 and #7). The first QCM (Part #6) is facing downward which monitors the $PbCl_2$ (received from Aldrich and used without further purification) evaporation rate while the second QCM (Part #7) facing upward is used to monitor the MAI vapor only. Two evaporation sources are needed for the perovskite film formation. Vapor of MAI is produced by a Knudsen cell (K-cell, Part #8) type source (KOD-Cell, Kitano Seiki) to fill the chamber. AlN crucibles containing MAI (1 cc volume) are resistively heated by applying current through a heating element which surrounds the crucible. The second component, $PbCl_2$ is resistively heated from a large dish-shaped crucible (Part #9) to provide large scale uniform evaporation. The heating element (Part #10) consists of a tungsten wire (ϕ=0.25 mm) wound into a spiral shape and connected to commercially available power supply (30 A/36 V) through electric feedthroughs (Part #11). The halide shutter (Part #12) is mounted on a linear motion device enabling independent calibration of the evaporation rate of MAI. The total pressure inside the chamber is monitored by a full-range ($1\times10^5 \sim 1\times10^{-7}$ Pa) pressure gauge (Crystal/Cold cathode gauge from R-DEC, Part #13).

Initially, the MAI QCM (Part#7) parameters were set to density (1.0 g/cm^3) and acoustic impedance (1.0) as reported previously [1, 2]. However, we were unable to calibrate our quartz crystal parameters (tooling factor) by the standard ways of measuring the thickness of deposited MAI film by AFM or profilometer. We have observed that MAI film growths as patches (islands) instead of a uniform flat film even on a flatter surface of silicon with native oxide. Thus, an alternative procedure similar to the one reported by Malinkiewicz *et al.* [3] and Polander *et al.* [4] has been conducted. Note that similarly they were also unable to determine the MAI thickness quantitatively in their systems. Our methodology is based on

the MAI vapor pressure inside the chamber. Because the QCM that monitors MAI faces upwards (Part#7) in our system, we set the QCM parameters so the signal-to-noise ratio was reasonable for monitoring the MAI during evaporation. The optimized parameters were ρ=0.2 g/cm^3; Z-factor = 0.2; Tooling = 100. Thus, the MAI QCM (Part#7) in our system also serves to monitor indirectly the MAI time evolution during heating and perovskite formation (see Fig. S2), but cannot quantify the absolute MAI amount inside the chamber. We have optimized the perovskite deposition conditions by preparing several batches of perovskite films prepared with a varied MAI nominal rates to identify the evaporation conditions that give strong diffraction peaks in X-ray diffraction (XRD, Fig. 2a) corresponding to the perovskite structure and at the same time give the minimal diffraction peak intensities for non-perovskite related phases (e.g. MAI).

The eventual excess of MAI on perovskites was observed to show detrimental device performance. Thus, we have analyzed carefully the possible origins for generating the non-stoichiometric perovskite films in our system and our methodology. The excess of MAI could be monitored by XRD measurements showing the characteristic 10° and 20° diffraction peaks. The following issues were detected as possible sources for generating excess of MAI in our system and were circumvented: (i) during the warm up of the MAI crucible until the nominal evaporation rate is attained, deposition of MAI on the substrate can occur. Although the sample shutter (Figs. 1 and S1, Part#5) is kept closed at all times until the perovskite deposition is started, the MAI was found to be volatile and thus, can deposit on the substrate. Our system was designed to have a load-lock chamber coupled to the hybrid deposition chamber and isolated by a gate-valve (10840-CE01, VAT). During warm up of the MAI and $PbCl_2$ crucibles, the sample holder carrying the large substrate (5×5 cm^2) is stored in the load-lock and avoids the MAI exposure. Only when the nominal rates are achieved, the sample holder is *in situ* transferred from the load-lock to the evaporation chamber by a magnetic transfer rod. The sample transfer operation takes less than 3 minutes; (ii) large variations of MAI pressure during perovskite deposition can generate sample with excess of MAI. A relatively high pressure of 0.3 Pa (~2.3 mTorr) is needed for the perovskite formation in our system. This high pressure is kept constant all the time during perovskite deposition by using the Knudsen-cell (Part#8, Fig. 1 and S1) that allows precise temperature control. In addition, the manual gate-valve (Part#2) is set to a predetermined opening position and minimum valve operation is required to keep the pressure (0.3 Pa) constant during perovskite deposition; (iii) The generation of the MAI vapor is not ceased immediately when the MAI heating element is

stopped because it takes a substantial period of time for the crucible to cool down. Thus, the remaining unknown concentration of MAI in the chamber generates perovskite films with topmost layers with different stoichiometric compositions (MAI:$PbCl_2$). After the completion of the deposition, the sample is immediately transferred from the deposition chamber to the load-lock chamber to minimize the excessive deposition of MAI on top of the perovskite films.

Methylammonium iodide synthesis. MAI was synthesized according to a literature procedure with slight modification [5]. Briefly, hydroiodic acid solution was gradually added to methyl amine ethanol solution that was kept stirring in an ice-bath. Ethanol and water from the mixed solution was evaporated using a rotary evaporator (BUCHI, Rotavapor R-3). The precipitated yellow-colored crystals were dissolved in hot ethanol, and cooled in a refrigerator at 5 °C for recrystallization. Subsequently, the crystals were filtered and washed with tetrahydrofuran resulting in white crystal powder. We dried and kept the MAI in N_2 glove box (<0.1 ppm of O_2 and H_2O).

Perovskite film deposition. The growth of perovskite films in our system is based on the concept of controlling the MAI vapor pressure and flow that fills the entire vacuum chamber. The K-cell (Part #8) produces well controllable amounts of the MAI vapor that is further controlled by the gate-valve (Part #2). A shutter in front of the K-cell is kept closed at all times to avoid the high flux of MAI hitting directly the substrate area. This is critical because the deposition only via MAI pressure ensures uniformity. Perovskite films are formed by a chemical reaction between the $PbCl_2$ deposited onto the substrate (that has good sticking coefficient, uniformity, wettability, and nicely forms the line-of-sight molecular beam according to the cosine law) and the MAI from the gas-phase (vapor). Because of the directionality nature of the lead halide deposition, the use of widely-open dish-shaped crucible surrounded by a spiral-shaped filament is essential for producing uniform evaporation rates of the lead halide across the entire substrate surface area. The high crystallinity through the entire film thickness is produced by a good control of the MAI vapor pressure and a stable lead halide evaporation rate. The gate-valve allows the control of the MAI vapor pressure inside the chamber (i.e., setting the gate-valve to a predetermined opening position can help hold the MAI vapor in the chamber during perovskite deposition) as well as to precisely stop the perovskite reaction at any time (by stopping the MAI heating

131 and opening completely the gate-valve). The substrates (5 cm × 5 cm in size) are loaded into
132 the temperature controlled holder stage and its temperature adjusted to 20°C. In addition, the
133 temperature of the chamber body is kept at ~70°C which helps to reduce the adsorption rate
134 of MAI on the chamber wall. In the case of conventional line-of-sight physical evaporation
135 method, the consumption of the MAI is much higher because the vapor of MAI is constantly
136 pumped out from the chamber. On the other hand, our hybrid deposition method implements
137 multiple measures that help not only maximize the efficient use of materials, but also
138 accelerate chemical reaction rate for the perovskite formation. It is anticipated that material
139 purity is essential for avoiding trap states and preventing exciton quenching [3] in solar cells.
140 In this aspect, the sublimation methods (and/or extensive outgassing) in vacuum chambers
141 are of particular advantage in preparing high purity perovskite films.
142 An in situ quadrupole mass spectrometry (QMS, Hiden HAL201) was conducted with
143 the aim to monitor MA and HI compounds during the sublimation of the MAI. Our QMS data
144 showed no evidence for the decomposition of MAI into MA and HI (below the detection
145 limit of our QMS). The m/z = 30, 31 and 127, 128 corresponding to the major signals of MA
146 and HI, respectively, were monitored while heating the MAI compound stepwise from room
147 temperature up to 150 °C.
148
149 **Perovskite film characterization and solar cell fabrication.** Perovskite films were
150 deposited on FTO glass pre-coated with a compact layer of TiO_2 (c-TiO_2) as reported
151 elsewhere [1, 6]. Multiple substrates (up to 9 in total) of 15×15 mm^2 in size were loaded into
152 the system. The substrates with the as-grown perovskite films were immediately transferred
153 to N_2 glove box for the complete device fabrication. The properties of the perovskite films
154 were studied by x-ray diffraction (XRD, D8 Bruker), atomic force microscope (AFM, MFP-
155 3D Asylum Research), and UV-vis (Evolution 600, Thermoscientific). The solar cell device
156 fabrication was completed by spin-coating a hole transport layer (HTM) that consists of a
157 mixture of three materials: spiro-MeOTAD (2,2',7,7'-tetrakis(N,N-di-p-methoxy-
158 phenylamine)-9,9'-spirobifluorene (Merck) dissolved in chlorobenzene (72.5 mg/mL), 17.5
159 μL of Li-bis(trifluoromethanesulfonyl)-imide (LiTFSI, Sigma) dissolved in acetronitrile (52
160 mg/100 μL), and 28.8 μL of tert-butylpyridine (*t*-BP, Sigma) [1, 6]. Finally, the Ag top
161 electrodes (100 nm) were deposited by thermal evaporation through a shadow mask defining
162 solar cell active areas of ~0.05 cm^2. Current-voltage device characteristics were measured by
163 applying an external potential bias under standard 1 sun AM1.5 simulated solar irradiation

(100 mW/cm^2, Newport Oriel Sol1A) and measuring the photocurrent generated (Keithley 2420 source meter). Typical voltage scan on our devices was performed starting from +1.1 V to −0.2 V (Forward). Prior to the first scan, pre-illumination under the solar simulator was performed for 30 seconds. It has been observed that more stable J-V curves with less hysteresis effects are obtained when the cells are illuminated prior to the J-V measurements. The scan rate was fixed at 0.15 V·s^{-1}. External quantum efficiency (EQE) was recorded as a function of wavelength on the complete devices (Newport Oriel IQE-200).

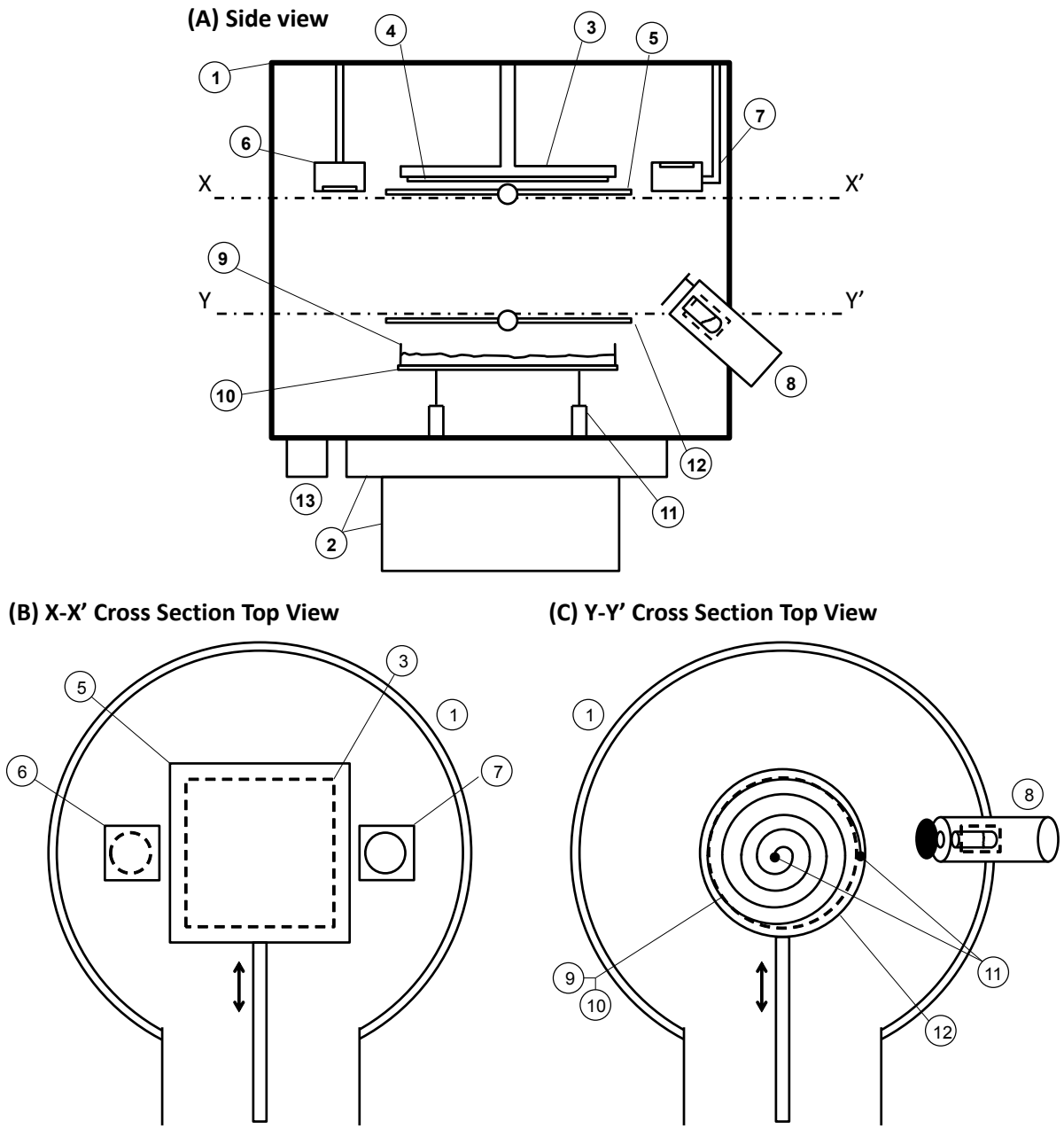

Figure S1. Side view of vacuum system for preparing highly crystalline large scale uniform perovskite films. Part numbers are defined as follows: (1) main vacuum chamber; (2) pumping system comprising a gate-valve and turbo molecular pump; (3) substrate holder stage allows cooling and heating from -190°C to 200°C; (4) substrate sizes up to 5×5 cm^2; (5) substrate shutter; Temperature controlled quartz crystal microbalance facing (6) downward and (7) upward; (8) Knudsen cell evaporator for producing MAI vapor-pressure; (9) widely opened dish-shaped crucible for the evaporation of lead halide compounds; (10) spiral-shaped tungsten wire; (11) electric feedthroughs; (12) lead halide shutter; (13) pressure gauge.

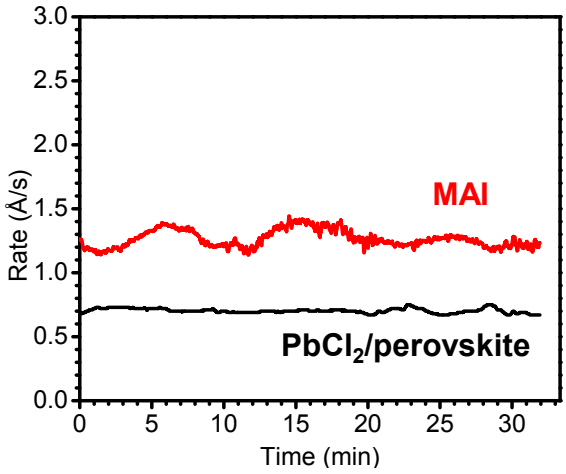

Figure S2. Typical time evolution of the evaporation rates observed in MAI (red curve) and $PbCl_2$ (black curve) quartz crystal microbalances (QCMs) during perovskite film deposition. The following values were used for setting the parameters in QCMs. $PbCl_2$ QCM (facing downward): ρ=5.85 g/cm^3; Z-factor = 0.8; Tooling = 70. MAI QCM (facing upward): ρ=0.2 g/cm^3; Z-factor = 0.2; Tooling = 100. Low density and Z-factor were chosen with the purpose to enhance the signal detection of MAI in QCM. The direct film calibration of MAI by means of AFM or profilometer was difficult because MAI film growths as small islands even on flatter substrates such as SiO_2(native oxide)/Si. Thus, the MAI partial pressure and rate were optimized by characterizing the final perovskite films formed by XRD. The good control of the MAI rate is inferred at a high pressure of ~0.3 Pa inside the chamber corresponding to 1.2–1.4 Å/s rate read in QCM.

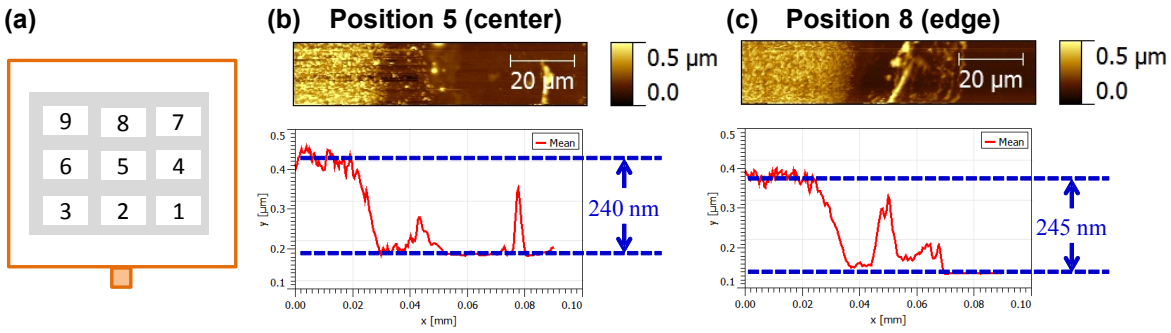

Figure S3. Tapping mode AFM images (scan size: 90 × 16 μm^2) showing the edge between perovskite film and substrate generated by covering half of the sample with a shadow mask. (a) Sample positions were numbered as indicated over the 5×5 cm^2 total area. AFM measurements were conducted (b) at the center and (c) at one edge on a large-scale 5×5 cm^2 area. The corresponding height-profiles (averaged across the vertical direction) are shown below the images (b) and (c).

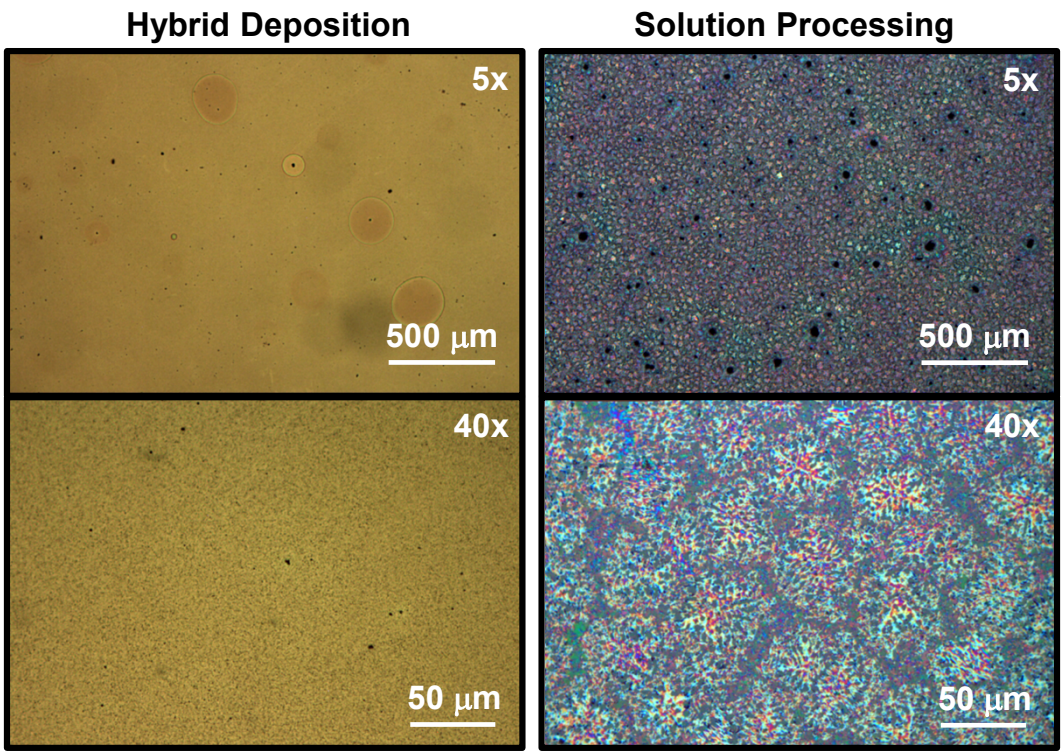

Figure S4. Optical microscope (Leica DM4000) images acquired on the ~135 nm perovskite film prepared by the hybrid deposition method (left column) and by the solution processing (right column). The solution processed perovskite film was prepared using the following procedure: MAI and $PbCl_2$ (Sigma-Aldrich) were dissolved in *N,N*-dimethylformamide with molar concentrations of 2.64 M and 0.88 M, respectively. The precursor solution was left stirring overnight to completely dissolve. 50 μL of perovskite precursor was spin-coated on the m-TiO_2/c-TiO_2/FTO at 2000 rpm for 30 seconds followed by a thermal annealing at 100°C for 45min. All sample preparation steps were conducted inside the N_2 glove box. The round-shaped features in the upper left corner image belong to the compact layer of TiO_2.

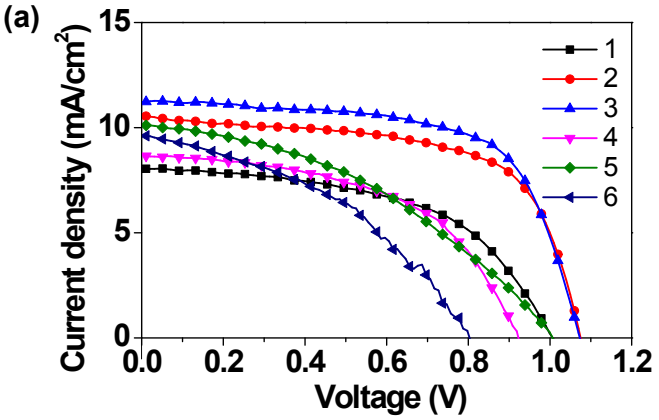

Device	V_{oc} (V)	J_{sc} (mA/cm^2)	FF	PCE (%)
1	1.01	8.06	53.23	4.32
2	1.06	9.85	56.88	5.92
3	1.05	10.75	56.23	6.37
4	0.93	8.69	51.76	4.17
5	1.00	10.10	40.39	4.09
6	0.80	9.74	41.36	3.21
Statistics	0.98±0.10	9.5±0.9	0.500±0.007	4.7±1.2

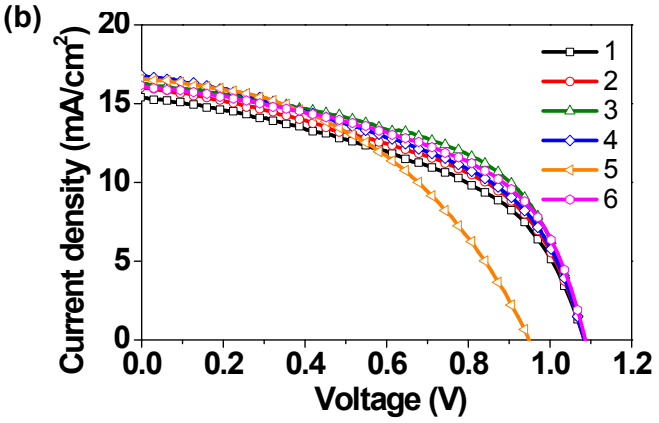

Device	V_{oc} (V)	J_{sc} (mA/cm^2)	FF	PCE (%)
1	1.084	16.06	47.82	8.32
2	1.085	16.72	48.83	8.85
3	1.086	16.98	53.49	9.86
4	1.085	16.04	47.73	8.30
5	0.951	15.86	44.41	6.69
6	1.085	15.39	51.90	8.67
Statistics	1.06±0.05	16.2±0.6	0.490±0.003	8.5±1.0

Figure S5. J-V characteristic curves on 6 devices of a FTO/c-TiO_2/perovskite/spiro-MeOTAD HTL/Ag solar cell measured under AM1.5G illumination. Perovskite film thicknesses are (a) ~50 nm and (b) ~135 nm.

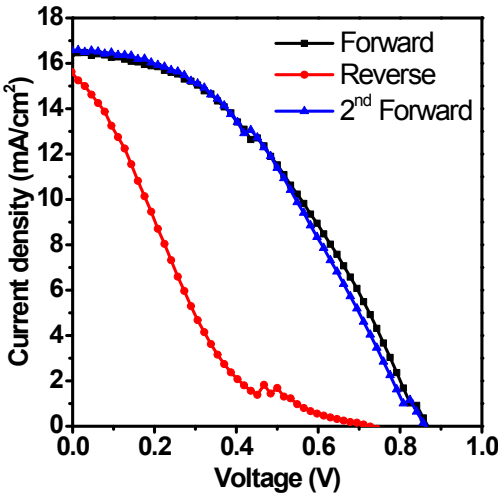

	V_{oc} (V)	Jsc (mA/cm^2)	Fill Factor	PCE (%)
Forward	0.871	16.39	40.47	5.78
Reverse	0.718	15.55	16.29	1.82
2nd Forward	0.862	16.50	40.63	5.78

Figure S6. J-V characteristic curves for a perovskite solar cell device measured under different scan direction showing the hysteresis. Three consecutive scans were performed at fixed scan rate of 0.15 V·s^{-1}. The voltage sweeping from high voltages to zero applied voltage and from zero voltage to high voltage are denoted as "Forward" and "Reverse", respectively.

The voltage sweeping from high voltages to zero applied voltage and from zero voltage to high voltage are denoted as "Forward" and "Reverse", respectively. We find that under the measurement conditions investigated here, higher PCEs are determined on all cells measuring from +1.1 V to –0.1 V ("Forward"). As comparison, a significant decrease in PCE of ~30% is determined going from –0.1 V to +1.1 V ("Reverse"). On the other hand, the perovskite films prepared by our method seem to be of high quality and uniformity over a large area, which is confirmed by multiple techniques. For example, our perovskite films showed high (110), (220), and (330) diffraction peaks in X-ray diffraction (XRD, Figs. 1b and 2a) over the 5×5 cm^2 substrate area. AFM images show extremely small morphology roughness over a scan area of 20 μm × 20 μm. The optical microscope images (Fig. S2) showed a very uniform coverage over the entire substrate. Therefore, we believe that the strong hysteresis effect is mainly caused by the selective contacts rather than perovskite films themselves [7]. The exact cause for the hysteresis features is not clear to us at the moment and this topic is still under investigation in our group.

References

[1] M.Z. Liu, M.B. Johnston, and H.J. Snaith, *Efficient planar heterojunction perovskite solar cells by vapour deposition.* Nature **501** (2013) 395-398.

[2] A.S. Subbiah, A. Halder, S. Ghosh, N. Mahuli, G. Hodes, and S.K. Sarkar, *Inorganic Hole Conducting Layers for Perovskite-Based Solar Cells.* J. Phys. Chem. Lett. **5** (2014) 1748-1753.

[3] O. Malinkiewicz, A. Yella, Y.H. Lee, G.M. Espallargas, M. Graetzel, M.K. Nazeeruddin, and H.J. Bolink, *Perovskite solar cells employing organic charge-transport layers.* Nat. Photonics **8** (2014) 128-132.

[4] L.E. Polander, P. Pahner, M. Schwarze, M. Saalfrank, C. Koerner, and K. Leo, *Hole-transport material variation in fully vacuum deposited perovskite solar cells.* APL Mater. **2** (2014) 081503.

[5] M.M. Lee, J. Teuscher, T. Miyasaka, T.N. Murakami, and H.J. Snaith, *Efficient Hybrid Solar Cells Based on Meso-Superstructured Organometal Halide Perovskites.* Science **338** (2012) 643-647.

[6] Q. Chen, H. Zhou, Z. Hong, S. Luo, H.-S. Duan, H.-H. Wang, Y. Liu, G. Li, and Y. Yang, *Planar heterojunction perovskite solar cells via vapor-assisted solution process.* J. Am. Chem. Soc. **136** (2013) 622-625.

[7] H.J. Snaith, A. Abate, J.M. Ball, G.E. Eperon, T. Leijtens, N.K. Noel, S.D. Stranks, J.T.-W. Wang, K. Wojciechowski, and W. Zhang, *Anomalous Hysteresis in Perovskite Solar Cells.* J. Phys. Chem. Lett. **5** (2014) 1511-1515.